



Textile Dye Removal by *Acacia dealbata Link.* Pollen Adsorption Combined with UV-A/NTA/Fenton Process

Ana R. Teixeira¹ · Nuno Jorge^{1,2} · José R. Fernandes³ · Marco S. Lucas¹ · José A. Peres¹

Accepted: 7 June 2022 / Published online: 13 July 2022
© The Author(s) 2022

Abstract

The decolourization of an aqueous solution of the textile dye Acid Red 88 (AR88) and the control of the invasive plant species *Acacia dealbata Link.* (ADL) were addressed in this work. The aims of the study were (1) characterization of the ADL pollen, (2) application of the pollen powder in adsorption processes, (3) selection of the best operational conditions for nitriloacetic acid (NTA)-UV-A-Fenton process and (4) assess the efficiency of the combined treatment adsorption and NTA-UV-A-Fenton in AR88 decolourization. In a first step, ADL pollen was used as a AR88 bioadsorbent. Fourier-transform infrared spectroscopy (FTIR) analysis were performed and revealed the presence of proteins, fatty acids, carbohydrates and lignin in the pollen. Afterwards, through scanning electron microscopy (SEM), it was possible to verify that ADL pollen has several empty spaces that can be used for dye adsorption. Biosorption results showed higher adsorption of AR88 with application of pH 3.0 and [pollen] = 3.0 g/L with 18.8 mg/g of dye adsorbed. The best fitting was observed with Langmuir, SIPS and Jovanovic isotherms (0.993, 0.996 and 0.994, respectively). To complement the biosorption, a UV-A-Fenton process was applied, and results showed a higher AR88 removal with (NTA) addition. Higher irradiance power favored the oxidation process with high Φ photodegradation value and low Electric Energy per Order (E_{EO}) and Specific Applied Energy (E_{SAE}). The combination of biosorption with NTA-UV-A-Fenton was the most efficient system with an AR88 decolourization of 98.5% and a total organic carbon (TOC) removal of 83.5%.

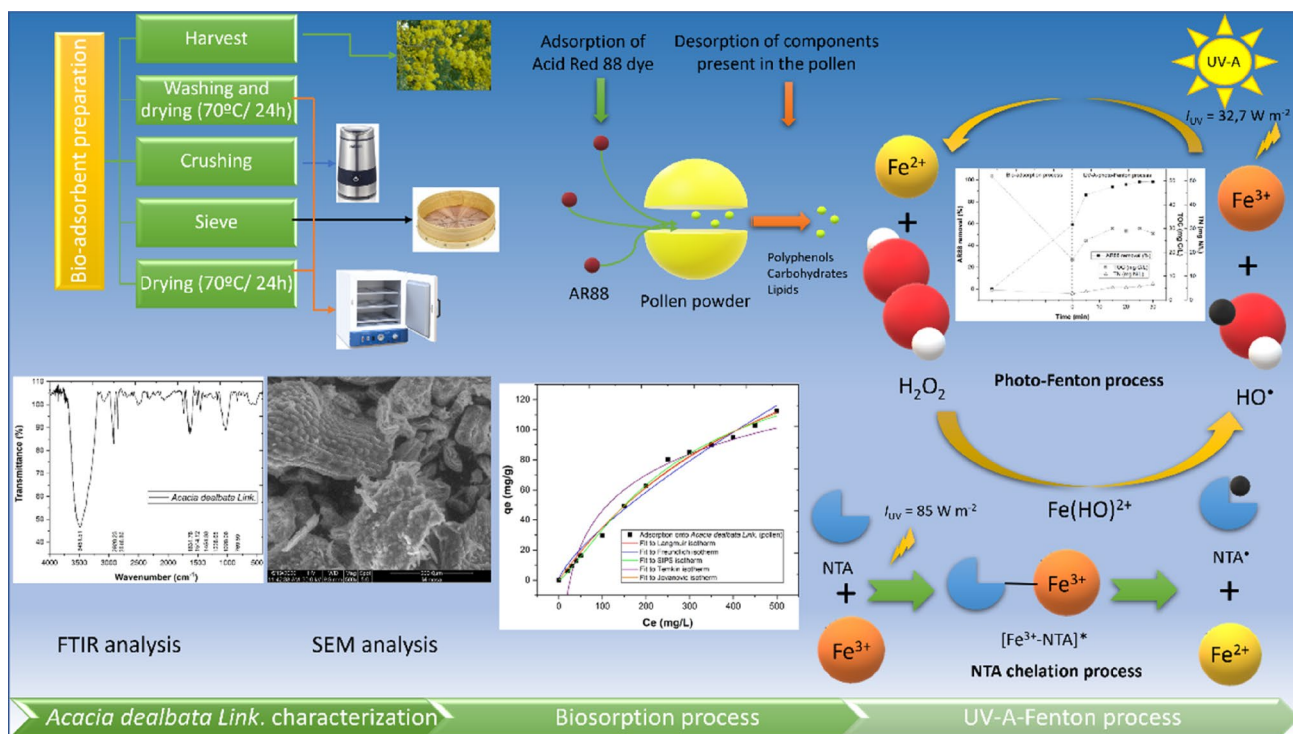
✉ Nuno Jorge
njorge@uvigo.es

¹ Centro de Química de Vila Real (CQVR), Departamento de Química, Universidade de Trás-os-Montes e Alto Douro (UTAD), Quinta de Prados, 5001-801 Vila Real, Portugal

² Escuela Internacional de Doctorado (EIDO), Campus da Auga, Campus Universitario de Ourense, Universidade de Vigo, As Lagoas, 32004 Ourense, Spain

³ Centro de Química de Vila Real (CQVR), Departamento de Física, Universidade de Trás-os-Montes e Alto Douro (UTAD), Quinta de Prados, 5001-801 Vila Real, Portugal

Graphical Abstract



Keywords Acid red 88 · Azo dye · *Acacia dealbata Link.* · Adsorption · Chelating agent · UV-A radiation

1 Introduction

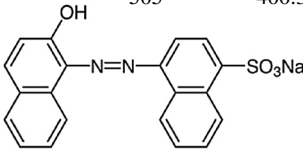
The textile industry has been one of the major polluters of surface and ground water resources because it uses as many as 8000 chemicals and huge amount of water. Several reports suggest that an average sized textile industry consumes about 1.6 million liters of water per day for the production of about 8000 kg of fabric [1, 2]. Among the textile dyes used, the acid red 88 (AR88) was selected to be studied in this work, because of its vast application in dyeing textile fabrics such as silk, nylon, wool and leather [3]. The azo dyes are not only toxic to the environment, but also mutagenic, teratogenic and carcinogenic chemicals [1] and therefore their elimination is a priority.

One treatment process that can be used for dye removal from wastewater is adsorption process. The adsorption process has attracted considerable attention due to its technical feasibility, flexibility and operation simplicity. Currently, the adsorbents that are widely used mainly include activated carbons [4], ion-exchange materials [5], zeolites [6] and bentonite clays [7, 8]. However, these adsorbents are still deemed expensive if applied to large-scale treatment of dye wastewater. To further decrease the cost, numerous new adsorbents have been developed from different bioresources

for dye removal. These bio-adsorbents have been considered promising due to the large availability and low cost of their raw materials [9]. One bio-resource in particular is the pollen powder of *Acacia dealbata Link.* (ADL), which is a native plant from Australia that became invasive species in Europe. Worldwide spread of *A. dealbata* increased more than 60% in the last decade [10]. In Portugal, the first record of the species is from 1850, when it was introduced for the cut-flower, tannin and timber industries [11, 12]. In a search performed in “Web of Science core collection”, it were observed the publication of 19,467 articles referent to “biosorption” and 102 articles referent to “*Acacia dealbata Link.*”, however, the combination of both terms revealed that no article has ever been published. Considering that ADL is an invasion plant, the use of its pollen for the adsorption of AR88 allows to solve two issues, the reuse of ADL and the removal of AR88.

Advanced oxidation processes (AOPs), such as photo-Fenton process can be efficient for the destruction of carbon-based contaminants. In literature, photo-Fenton process has been used for treatment of emerging contaminants [13], phenolic compounds [14], textile dyes [15, 16], pharmaceuticals [17], among others. In the photo-Fenton process, the ultra-violet (UV) light can assist the reduction of Fe³⁺ to Fe²⁺ to

Table 1 Chemical structure, adsorption maxima and molecular weight of AR88

Name	Chemical structure	λ_{\max} (nm)	Molar mass (mol g ⁻¹)	Reference
Acid red 88 (acid dye)		505	400.38	[23]

react with H₂O₂ to generate HO[•] radicals. In view of this, UV-Light-emitting diodes (LEDs) lamps, are efficient and ecofriendly, they do not over heat, they have a long lifetime and low energy consumption [18, 19].

The photo-Fenton process is affected by some operational parameters, including the concentration and ratio of Fenton's reagent (H₂O₂ and Fe²⁺), solution pH, time, temperature, pollutant concentration and the nature of reaction matrix [20]. The use of chelating agents, such as nitriloacetic acid (NTA) can help to overcome these disadvantages, because (i) they promote the activation of hydrogen peroxide and the generation of HO[•] radicals (ii) they improve the solubility of nonpolar and lipophilic pollutants (iii) they enhance the dissolution of iron at neutral pH and allow the reduction of Fe³⁺ to Fe²⁺ using UV light (iv) chelates have the ability to form higher quantum yield from HO[•] as compared to other Fe³⁺-complexes (v) finally, when chelates are used, wider range of solar radiation spectrum can be applied in photo-Fenton system [21, 22].

To our knowledge, biosorption with ADL pollen powder was never performed for the treatment of AR88 and the UV-A/NTA/Fenton system was never applied for AR88 removal, therefore, there are many variables that require further studies. Therefore, the aim of this work is (1) harvest and characterize ADL pollen, (2) study the effect of variables pH, ADL dosage and AR88 concentration in the biosorption efficiency, (3) optimize the UV-A-NTA-Fenton process, (4) study the combined effect of biosorption and UV-A-Fenton processes.

2 Materials and Methods

2.1 Reagents

The acid dye, Acid Red 88 (Color Index 15620), chemical formula C₂₀H₁₃N₂NaO₄S was provided by Aldrich Chemical Company, Inc., Milwaukee, USA and used as received without further purification. The molecular structure of AR88 in non-hydrolyzed form is illustrated in Table 1. The iron (II)

sulfate heptahydrate (FeSO₄·7H₂O) was acquired by Pan-reac, Barcelona, Spain, the hydrogen peroxide (H₂O₂ 30% w/w) and nitriloacetic acid (C₆H₉NO₆, NTA) were supplied by Sigma-Aldrich, Missouri, USA. For pH adjustment, it was used sodium hydroxide (NaOH) from Labkem, Barcelona, Spain and sulphuric acid (H₂SO₄, 95%) from Scharlau, Barcelona, Spain. Deionized water was used to prepare the respective solutions.

2.2 Bio-adsorbent Preparation

The pollen from the plant ADL used on this work was collected on the district of Vila Real (Portugal) and transported to the Environmental Engineering Laboratory of the University of Trás-os-Montes and Alto Douro, Vila Real, where it was stored until used. This specie was collected at the GPS location 41°17'12.9"N 7°44'14.1"W on March 2021. The pollen was washed and dried in an incu-line incubator, VWR, V. Nova de Gaia, Portugal at 70 °C for 24 h. Then they it was grounded into powder using a groundnut miller. The grounded powder was then sieved to a mesh size of 150 µm. Finally, the powder was once more dried at 70 °C for 24 h to remove the moisture. The powder was then left to cool and stored in a tightly closed plastic jar.

2.3 Bio-adsorbent Characterization

The Fourier-transform infrared spectroscopy (FTIR) spectra was obtained by mixing 2 mg of pollen with 200 mg KBr. The powder mixture was then inserted into the molds and pressed at 10 ton/cm² to obtain the transparent pellet, which was analyzed with an IRAffinity-1S Fourier Transform Infrared spectrometer (Shimadzu, Kyoto, Japan) and the infrared spectra in transmission mode were recorded in the 4000–400 cm⁻¹ frequency region. The microstructural characterization was carried out with a scanning electron microscopy (FEI QUANTA 400 SEM/ESEM, Fei Quanta, Hillsboro, WA, USA). The mineral characterization (iron, copper, sodium, potassium, calcium and magnesium) was obtained by digestion of 500 mg of pollen by nitric acid and hydrogen peroxide for 24 h. Then the samples were transferred to a Dry Block Heater reactor (Techne, Cole-Parmer, UK), at 60 °C. The temperature was gradually raised to 80, 100, 120 and 150 °C, then the samples were cooled, and finally a matrix solution (1.5 mL de HNO₃ p.a. conc. in 1000 mL distilled water) was added. In a final step, the cations concentrations were analyzed by atomic absorption spectroscopy (AAS) using a Thermo Scientific™ iCE™ 3000 Series (Thermo Fisher Scientific, Massachusetts, USA).

2.4 Biosorption Experimental Setup

The biosorption of AR88 contaminant from the aqueous solution by the organic adsorbent *Acacia dealbata* Link. pollen powder (ADL) was studied in detail, in order to predict the amount of AR88 removed through adsorption process. The adsorption process was performed under constant agitation of a 75 mL aqueous solution, by a L32 Basic Hotplate Magnetic Stirrer (Labinco, Breda, Netherlands). The pollen was added to the aqueous solution and the samples were withdrawn at time 0, 5, 10, 15, 20, 25 and 30 min (Fig. 1). The biosorption batch experiments were carried out in three different steps, under fixed conditions ($T=298$ K, $V=75$ mL, agitation = 350 rpm, $t=30$ min):

1. variation of the pH conditions (3.0–9.0), with $[AR88]=50$ mg L⁻¹, $[pollen]=3.0$ g L⁻¹;
2. variation of the pollen dosage (1.5–10 g L⁻¹), with pH 3.0, $[AR88]=50$ mg L⁻¹;
3. variation of the contaminant AR88 concentration (0–500 mg L⁻¹), with pH 3.0, $[pollen]=3.0$ g L⁻¹.

After the adsorption process, the samples were centrifuged and separated for subsequent chemical analysis. Then, 2 mL of dye solution was withdrawn and analyzed in a UV–Vis scanning spectrum 200–800 nm, using a Jasco V-530 UV–Vis spectrophotometer (Tokyo, Japan). The maximum absorbance wavelength (λ_{max}) of AR88 was found at 505 nm, and the concentration of the residual dye in solution was calculated

by Beer-Lambert's law, using the optical density and molar extinction observed at the characteristic wavelength [16].

Prior to the measurement, a calibration curve was obtained by using Acid Red 88 solution at known concentrations. The percentage of dye removal was calculated as follows (Eq. 1) [24]:

$$\text{Dye degradation(\%)} = \left(\frac{C_{\text{dye},0} - C_{\text{dye},t}}{C_{\text{dye},0}} \right) \times 100 \quad (1)$$

where $C_{\text{dye},t}$ and $C_{\text{dye},0}$ are the concentrations of dye at reaction time t and 0, respectively.

The amount of AR88 adsorbed was calculated according to Eq. 2 [25, 26], as follows:

$$q_e = \frac{(C_0 - C_e) \times V}{m} \quad (2)$$

where q_e is the adsorption capacity at adsorption equilibrium (mg g⁻¹), C_0 and C_e are the concentration of AR88 at time 0 and t , V is the volume (L) and m the mass of adsorbent (g).

2.5 Isothermal Models

The mechanism of the adsorption process was investigated through the fit of the experimental data to different adsorption isotherms, based on Langmuir, Freundlich, SIPS, Temkin and Jovanovic [27–32]. Table 2 resumes the isotherm equations used in this study. The goodness

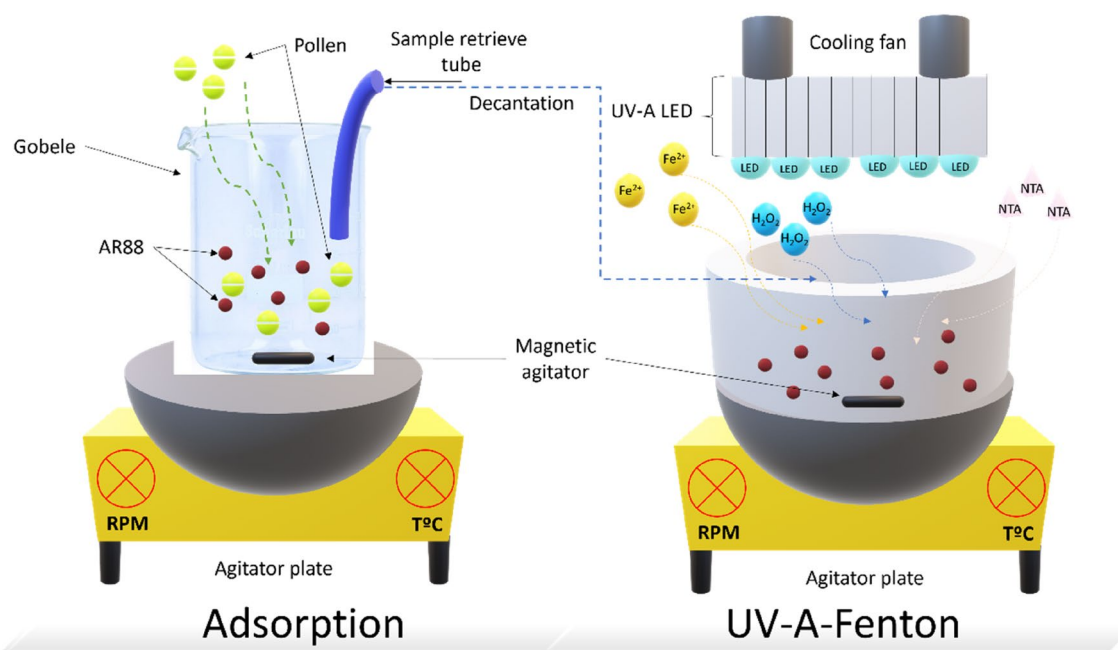


Fig. 1 Schematic setup of adsorption and UV-A-Fenton process

Table 2 Nonlinear form of isotherm equations used to fit the adsorption data

Model/equation	Parameters	References
Langmuir $q_e = \frac{q_m K_L C_e}{1 + K_L C_e}$	q_e (mg g ⁻¹)—equilibrium adsorption capacity q_m (mg g ⁻¹)—maximum adsorption capacity K_L (L g ⁻¹)—Langmuir constant C_e (mg L ⁻¹)—equilibrium adsorbate concentration in solution	Langmuir [27]
Freundlich $q_e = K_F C_e^n$	K_F (mg g ⁻¹ (mg L ⁻¹) ⁻ⁿ) —Freundlich constant n —heterogeneity factor	Gustafsson et al. [28]
SIPS $q_e = \frac{q_m K_S C_e^n}{1 + K_S C_e^n}$	K_S (L kg ⁻¹)—SIPS constant	Maurer [33] and Jeppu and Clement [34]
Temkin $q_e = \beta \times \ln K_T + \beta \times \ln C_e$	β (J mol ⁻¹)—Temkin constant	Wibowo et al. [29]
Jovanovic $q_e = q_m [1 - \exp(-b \times C_e)]$	b (L g ⁻¹)—binding constant	Jovanovic [32]

of fit of different regression models was evaluated by the correlation coefficient R².

2.6 Photo-Fenton Experimental Setup

The photo-Fenton process was carried out in a lab-scale batch reactor, which was illuminated with a UV-A LED photo-system (Fig. 1). The photo-system consisted by a matrix of 12 InGaN LEDs lamps (Roithner APG2C1-365E LEDs) with a maximum emission wavelength at $\lambda = 365$ nm. The nominal consumption of each LED lamp was 1.4 W at an applied current of 350 mA. The radiation is emitted in continuous mode for all the 12 UV-A LEDs, being controlled by a power MOSFET in six different current settings, resulting in irradiance levels (I_{UV}) from 16 up to 85 W m⁻² measured at 5 cm distance with a UVA Light Meter (Linsang model LS126A). For every experiment performed, the reactor was initially loaded with 250 mL of Acid Red 88 (AR88) aqueous solution, under constant agitation by means of a L32 Basic Hotplate Magnetic Stirrer 20 L (Labinco, Breda, Netherlands).

The photo-Fenton process was optimized as follows, by maintaining fixed conditions of temperature = 298 K, agitation 350 rpm and t = 30 min:

1. Performance of H₂O₂ variation (2–16 mM), pH 3.0, [Fe²⁺] = 0.15 mM, [AR88] = 50 mg L⁻¹ radiation UV-A (365 nm), $I_{UV} = 32.7$ W m⁻²;
2. Performance of Fe²⁺ variation (0.05–0.20 mM), pH 3.0, [H₂O₂] = 4 mM, [AR88] = 50 mg L⁻¹ radiation UV-A (365 nm), $I_{UV} = 32.7$ W m⁻²;
3. Performance of NTA variation (0.05–0.20 mM), pH 3.0, [H₂O₂] = 4 mM, [Fe²⁺] = 0.15 mM,

- [AR88] = 50 mg L⁻¹ radiation UV-A (365 nm), $I_{UV} = 32.7$ W m⁻²;
4. Performance of [AR88] variation (25–100 mg L⁻¹), pH 3.0, [H₂O₂] = 4 mM, [Fe²⁺] = 0.15 mM, [NTA] = 0.10 mM, radiation UV-A (365 nm), $I_{UV} = 32.7$ W m⁻²;
5. Performance of pH variation (3.0–7.0), [H₂O₂] = 4 mM, [Fe²⁺] = 0.15 mM, [NTA] = 0.10 mM, [AR88] = 50 mg L⁻¹ radiation UV-A (365 nm), $I_{UV} = 32.7$ W m⁻²;
6. Performance of irradiance power variation ($I_{UV} = 0 - 32.7$ W m⁻²), pH 3.0, [H₂O₂] = 4 mM, [Fe²⁺] = 0.15 mM, [NTA] = 0.10 mM, [AR88] = 50 mg L⁻¹ radiation UV-A (365 nm).

After the reaction has started, 2 mL of dye solution was withdrawn at periodic intervals and analyzed in a UV–Vis scanning spectrum 200–800 nm, using a Jasco V-530 UV–Vis (Tokyo, Japan). The samples were filtrated by 0.20 μ m filter and the ferrous ion (Fe²⁺) concentrations were analyzed by atomic absorption spectroscopy (AAS) using a Thermo Scientific™ iCE™ 3000 Series (Thermo Fisher Scientific, Massachusetts, USA). Total Organic Carbon (TOC) and Total Nitrogen (TN) samples were analyzed by direct injection of filtered samples into a Shimadzu TOC-L_{CSH} analyzer (Shimadzu, Kyoto, Japan), equipped with an ASI-L autosampler, provided with an NDIR detector and calibrated with standard solutions of potassium phthalate, hydrogen peroxide concentration was followed, using titanium (IV) oxysulfate (DIN 38 402H15 method) at 410 nm, using a portable spectrophotometer from Hach (Loveland, Colorado, USA).

In all the experiments, AR88 removal followed pseudo first-order kinetics, as follows (Eq. 3) [35], as follows:

$$r = -\frac{dAR88}{dt} = k_m AR88 \quad (3)$$

where r is the reaction rate, AR88 is the concentration of Acid Red 88 (mg/L) at time t and k_m is the pseudo first-order mineralization-rate constant. This equation can be integrated between times $t=0$ and $t=t$ to yield (Eq. 4), as follows:

$$\ln \frac{AR88_0}{AR88_t} = k_m t \quad (4)$$

According to this expression, a plot of the first term versus t must yield a straight line satisfying Eq. 4, where the slope is k_m [36].

As the oxidation reaction proceeds, the concentration of the reactant(s) decreases. Another measure of the rate of a reaction, relating concentration to time, is the half-life ($t_{1/2} = 0.693/k$) which is the time required for the concentration of a reactant to decrease to half of its initial concentration [35].

2.7 Figures of Merit E_{EO} and E_{SAE}

The figure-of-merit electric energy per order (E_{EO}) [37, 38] was used to evaluate the efficiency of the UV-A radiation in the degradation of AR88 by photo-Fenton process (Eq. 5), as follows:

$$E_{EO} = \frac{P \times t \times 1000}{V \times \log\left(\frac{C_i}{C_f}\right)} \quad (5)$$

where P is the rated power (kW) of the system, V is the volume (L) of water treated in time t (h), C_i and C_f are the initial and final concentrations, and the factor of 1000 converts g to kg. A more practical equation can be derived assuming first order kinetics and converting the units of the first order kinetic constants to min^{-1} , which results in Eq. 6 [37, 39], as follows:

$$E_{EO} = \frac{38.4 \times 10^{-3} \times P}{V \times k_{\text{obs}}} \quad (6)$$

Equation 6 can be further modified into Eq. 7, to represent the Specific Applied Energy (E_{SAE}) i.e. the energy required for breaking 1 mol of pollutant.

$$E_{SAE} = \frac{E_{EO}}{C_0 \times 10^3} \quad (7)$$

where C_0 is the initial pollutant concentration (mol L^{-1}).

All the experiments were performed in triplicate, and statistical analysis was performed using one-way analysis of variance (ANOVA) and differences were considered as significant when $p < 0.05$. The average values were compared using Tuckey's test, with OriginLab 2019 software

(Northampton, MA, USA). All data present mean and standard deviation (mean \pm SD).

3 Results and Discussion

3.1 Characterization of ADL Pollen

An initial analysis to the ADL (pollen powder), revealed a low concentration of iron and copper (1.6 and 0.4 mg L^{-1} , respectively), and high concentrations of sodium, potassium, calcium and magnesium (99.5 , 777.4 , 94.8 and 74.9 mg L^{-1} , respectively). Calcium and magnesium are important plant nutrients and play roles in stress resistance and photosynthesis in ADL plants. Calcium signaling is an important effector of cellular senescence [40]. The iron and copper concentrations were observed to be very low regarding the other ions. Iron and copper are essential trace elements for plants, being involved in many processes of metabolisms [41, 42], however an excess concentration can result in toxicity, especially in altering chromatin structure, synthesis of chlorophyll and protein, enzyme activity, photosynthesis and respiration, water content and plant biomass yield [43, 44].

Figure 2 shows the FTIR analysis of ADL (pollen). It is observed an adsorption broad band at 3481.51 cm^{-1} , which indicated the presence of the phenolic hydroxyl groups (OH stretching vibrating) [45], proteins, fatty acids, carbohydrates and lignin [46]. The 2920.23 and 2848.86 cm^{-1} absorption bands were attributed to C–H and CH_2 vibrations of aliphatic hydrocarbon. The 1631.78 , 1514.12 and 1454.33 cm^{-1} absorption bands indicated the presence of aromatic ring stretching vibration [45, 47]. The 1028.06 cm^{-1} absorption band was attributed to C–O stretching vibration from the

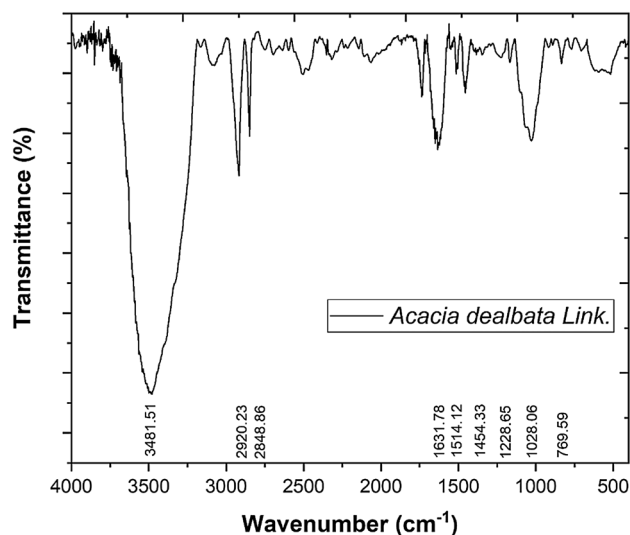


Fig. 2 FTIR spectra of ADL pollen powder

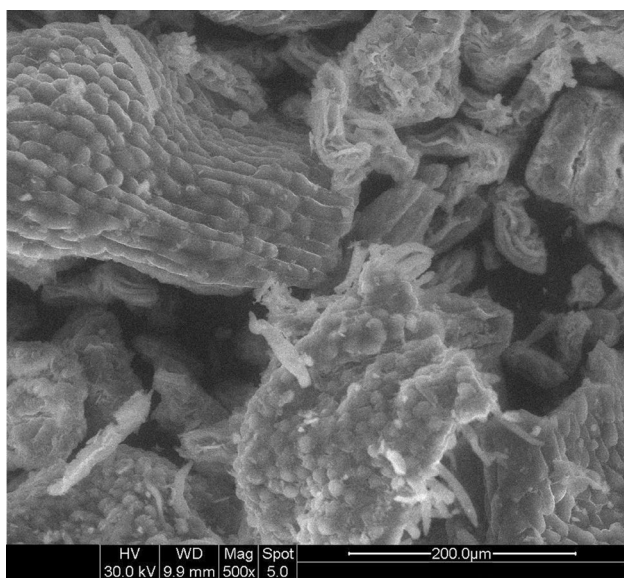


Fig. 3 Scanning electron microscopy (SEM) images of the ADL pollen with high magnification (500×)

glucose ring vibration and the holocellulose and hemicellulose [45, 47, 48]. From 1200.00 to 1000.00 cm^{-1} absorption bands, it was included the C–O–C symmetrically stretching vibration and the aromatic C–H in-plane bending vibrations [48].

In Fig. 3 it is observed the SEM image of the ADL pollen powder used as a bio-adsorbent in this study. This figure also shows that pollen particles have a heterogeneous structure with an irregular surface. The morphology of the pollen particles can potentially facilitate the adsorption process. In addition, the structure facilitates the process of ion adsorption due to the interstices and to the presence of protein components in the pollen [49]. Also, in accordance to Boulaadjoul et al. [50] and Araujo et al. [51] chainlike and spherical structures contributed to lowering the turbidity and color in the wastewater.

3.2 Adsorption of Acid Red 88 Experiments

3.2.1 Influence of pH Variation

The pollen presents a pH in water of 5.68 ± 0.04 . Considering that the pH presents an important factor for adsorption, in this section, the pH of the AR88 aqueous solution was varied (from 3.0 to 9.0), under the following conditions: $[\text{AR88}] = 50 \text{ mg L}^{-1}$, $[\text{pollen}] = 3.0 \text{ g L}^{-1}$ $T = 298 \text{ K}$, $V = 75 \text{ mL}$, $\text{agitation} = 350 \text{ rpm}$, $t = 30 \text{ min}$. Figure 4 shows a high amount of AR88 adsorbed at pH 3.0, 4.0, 5.0 and 6.0 ($16.3, 16.0, 15.9$ and $15.7 \text{ mg g}^{-1}_{\text{pollen}}$, respectively). From this point onward, it was observed a significant decrease of

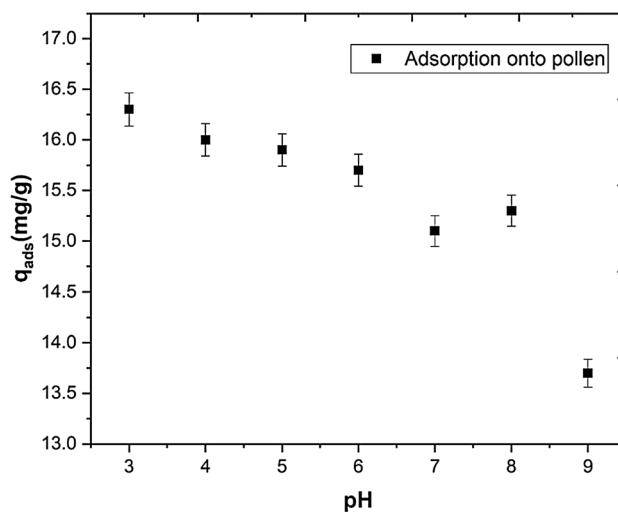
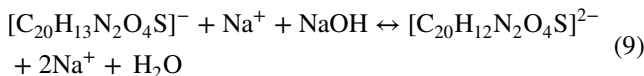
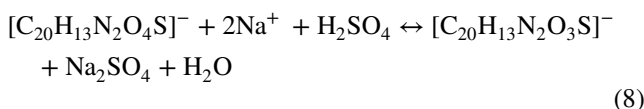


Fig. 4 Biosorption of textile dye AR88 from aqueous solution onto pollen powder at different pH conditions (3.0–9.0). Operational conditions: $[\text{AR88}] = 50 \text{ mg L}^{-1}$ $[\text{pollen}] = 3.0 \text{ g L}^{-1}$ $T = 298 \text{ K}$, $V = 75 \text{ mL}$, $\text{agitation} = 350 \text{ rpm}$, $t = 30 \text{ min}$

the amount adsorbed to $15.1 \text{ mg/g}_{\text{pollen}}$ (pH 7.0), followed by a higher decrease to $13.7 \text{ mg/g}_{\text{pollen}}$ (pH 9.0).

These results can be explained due to the fact that the biosorption processes primarily at pH of 3–5 for the carboxylic group [52]. At acidic pH, it is observed the cationic form of the pollen, which should be higher at acidic pH and lower at basic level. The electrostatic attraction between pollen cationic chains and negatively charged anions in the dye molecules, was then reinforced and the links to hydrophobic chains were enhanced [53]. At neutral pH, relatively low adsorption of AR88 by pollen was observed because HO^- could compete with the dye anions for sorption sites [54]. Equations 8 and 9 shows the reactions of AR88 with H_2SO_4 and NaOH .



These results are in agreement to the work of Buvaneswari and Kannan [55], who observed a higher adsorption capacity of dyes on brinjal plant root powder (cellulose) at pH range from 2.0 to 5.0. Considering these results, pH 3.0 was selected as the best pH for adsorption of AR88 by pollen.

3.2.2 Variation of Pollen Dosage

In the previous section, it was observed that pH had a significant influence in biosorption process. In this section, the influence of pollen dosage on adsorption capacity was investigated. The dosage of pollen was varied from 1.5 to 10 g/L under the following conditions: pH = 3.0, [AR88] = 50 mg L⁻¹, T = 298 K, V = 75 mL, agitation = 350 rpm, t = 30 min. An increase of the pollen dosage from 1.5 to 10 g L⁻¹ did not represent an increase of AR88 removal (97.1 and 95.0%, respectively). These results were due to the fact that with the application of 1.5 g L⁻¹ pollen, a high number of valuable adsorption sites were available, leading to a high AR88 removal, and therefore, the increase of pollen dosage was expected to achieve similar values in AR88 removal. For another hand, the mass of AR88 adsorbed per gram of adsorbent has decreased from 32.4 mg g⁻¹ (1.5 g L⁻¹ pollen) to 16.3, 8.0 and 4.8 mg g⁻¹, respectively, for 3.0, 6.0 and 10 g L⁻¹ pollen (Fig. 5), showing a decline in the removal efficiency as increasing of pollen dosage. Therefore, it was found inviable, the use of dosages higher than 3.0 g L⁻¹, and considering the AR88 adsorbed, the pollen dosage of 3.0 g L⁻¹ was selected for the following step.

3.2.3 Influence of Initial AR88 Concentration–Adsorption Isotherms

After the variation of pH and pollen dosage, the variation of contaminant concentration (AR88 concentration) was also studied in the adsorption process. The AR88 concentration

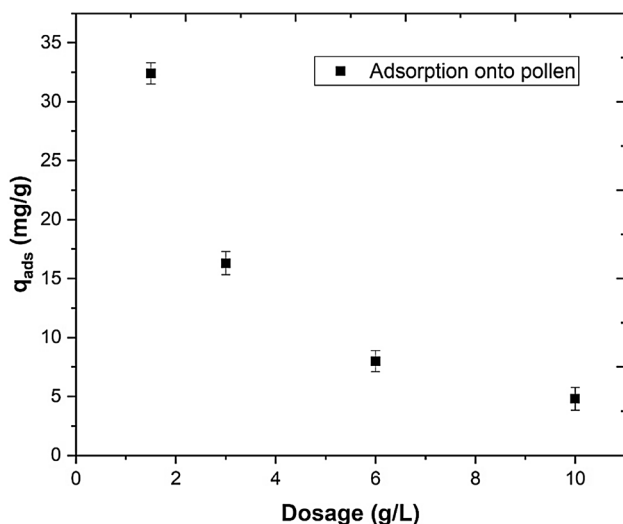


Fig. 5 Biosorption of textile dye AR88 from aqueous solution onto pollen powder at different dosage (1.5–10 g L⁻¹). Operational conditions: pH 3.0, [AR88] = 50 mg L⁻¹, T = 298 K, V = 75 mL, agitation = 350 rpm, t = 30 min

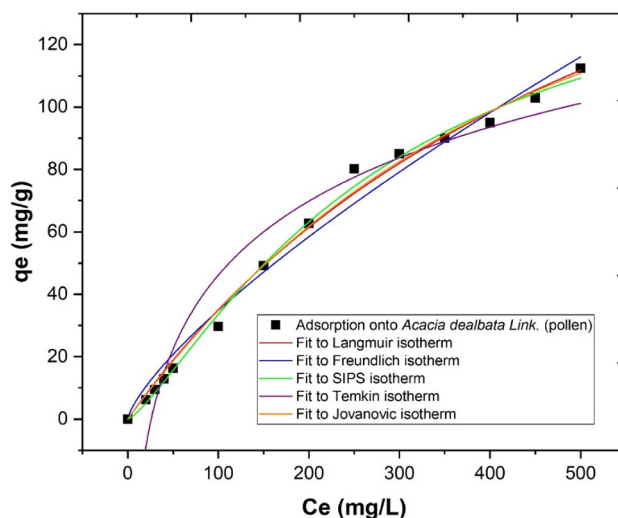


Fig. 6 Adsorption isotherm describing the amount of AR88 contaminant adsorbed onto pollen as a function of AR88 concentration (0–500 mg L⁻¹). Operational conditions: pH 3.0, [pollen] = 3.0 g L⁻¹, T = 298 K, V = 75 mL, agitation = 350 rpm, t = 30 min

was varied from 0 to 500 mg/L under the fixed conditions, as follows: pH = 3.0, [pollen] = 3.0 g L⁻¹, T = 298 K, V = 75 mL, agitation = 350 rpm, t = 30 min. The isothermal curve corresponding to the variation of the amount adsorbed (q_e) as a function of the equilibrium AR88 concentration is shown in Fig. 6. In this step, an increase of the amount of AR88 adsorbed was observed (6.2 to 112.4 mg g⁻¹), with the increase of the equilibrium AR88 concentration, which suggested that the gradient of concentration acted as an

Table 3 Isothermal parameters obtained from the fit of different isothermal models to pollen powder adsorption data

Isothermal model	Model parameters	Pollen adsorption
Langmuir	q_{\max} (mg g ⁻¹)	246
	K_L (L g ⁻¹)	1.66×10^{-3}
	r^2	0.993
Freundlich	K_f (mg g ⁻¹ (mg L ⁻¹) ⁻ⁿ)	1.11
	n	0.748
	r^2	0.985
SIPS	K_s	3.57×10^{-3}
	q_m (mol kg ⁻¹)	161
	n	1.29
Temkin	r^2	0.996
	K_t (L g ⁻¹)	3.86×10^{-2}
	β (J mol ⁻¹)	34.2
Jovanovic	r^2	0.958
	q_m (mg g ⁻¹)	152
	b (L g ⁻¹)	2.6×10^{-3}
	r^2	0.994

increasing driving force resulting into additional sorption capacity [56].

Different adsorption isothermal models were used in analyzing the experimental data obtained and fitted to the equilibrium sorption data of acid red 88 dye. In accordance with Table 3, Langmuir, SIPS and Jovanovic isotherms provided the best fitting to the sorption data, considering the correlation coefficients (0.993, 0.996 and 0.994, respectively). As observed for Langmuir model, Jovanovic model also assumes a homogeneous adsorption onto energetically homogeneous sorption sites. However, Jovanovic model was developed to describe the adsorption in solid phases, and considers additional interactions between the adsorbed molecules and the bulk phase [32, 57]. In addition, Jovanovic model predicts a maximum adsorption capacity, as the saturation point approaches, which in this case corresponds to 152 mg/g. The binding constant (b) measures the adsorption affinity and corresponds to $2.6 \times 10^{-3} \text{ L g}^{-1}$. The SIPS isotherm resulted from the Freundlich and Langmuir isotherms, and provided the best fitting of the experimental results. In Table 3, it is observed the value of $n = 1.29$, and in accordance to Broom [58], SIPS isotherm is reduced to Langmuir isotherm when $n \approx 1$, thus confirming the homogeneity of the adsorbent.

These results allowed a better understanding about the removal capacity of textile dyes through adsorption by biologic agents. Considering the adsorption results obtained in this section, a set of experimental conditions, namely, pH 3.0, [AR88] = 100 mg L^{-1} , [pollen] = 3.0 g L^{-1} , T = 298 K, V = 75 mL, agitation = 350 rpm, t = 30 min, were selected to perform combined biosorption/UV-A-Fenton process.

3.3 UV-A-Fenton Experiments

3.3.1 Assessment of Different AOPs in the Degradation of AR88

In order to degrade the AR88, it was necessary to understand which were the best oxidation processes. Therefore, in this section it were conducted several trials: (1) H_2O_2 , (2) UV-A, (3) UV-A + H_2O_2 , (4) UV-A + Fe^{2+} , (5) Fenton, (6) UV-A-Fenton. From the results obtained (Fig. 7), it is possible to observe that AR88 was resistant to degradation by application of H_2O_2 , UV-A, UV-A + H_2O_2 and UV-A + Fe^{2+} . Clearly, the oxidation potential of these processes is insufficient to promote the degradation of AR88 and, therefore, no generation of hydroxyl radicals (HO^\cdot) takes place. With the Fenton and UV-A-Fenton process it was observed a higher AR88 removal (63.1 and 91.4%, respectively). The Fenton process achieves an AR88 removal due to a high production of HO^\cdot radicals, however, the conversion of Fe^{3+} to Fe^{2+}

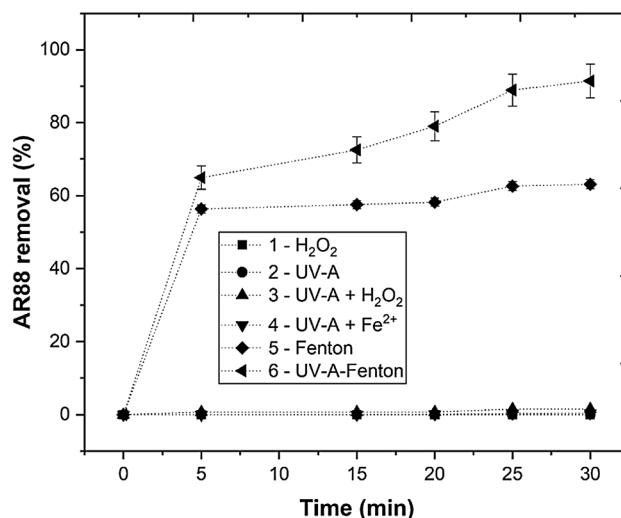


Fig. 7 Assessment of different AOPs in the degradation of AR88 under operational conditions as follows: pH 3.0, $[\text{H}_2\text{O}_2] = 4 \text{ mM}$, $[\text{Fe}^{2+}] = 0.15 \text{ mM}$, $[\text{NTA}] = 0.10 \text{ mM}$, agitation 350 rpm, T = 298 K, radiation UV-A (365 nm), $I_{\text{UV}} = 32.7 \text{ W m}^{-2}$, t = 30 min

is low making its efficiency limited. With the application of UV-A radiation, this limitation is overcome, because the UV radiation regenerates the Fe^{3+} to Fe^{2+} . The $\text{Fe}(\text{HO})^{2+}$ ion shows absorption bands between $290 \text{ nm} < \lambda < 400 \text{ nm}$, which allows the use of UV-A radiation and promotes the increase of HO^\cdot radicals in comparison to Fenton process alone, as observed in Eq. 10 [59].



Considering the high removal results of UV-A-Fenton, in the next steps this AOP will go through a series of parameters variation in order to reach the best operational conditions.

3.3.2 Influence of H_2O_2 Concentration

In this section, it was varied the H_2O_2 concentration (2–6 mM), under the following operational conditions: pH 3.0, $[\text{Fe}^{2+}] = 0.15 \text{ mM}$, $[\text{AR88}] = 50 \text{ mg L}^{-1}$, agitation 350 rpm, T = 298 K, radiation UV-A (365 nm), $I_{\text{UV}} = 32.7 \text{ W m}^{-2}$, t = 30 min. The results showed an AR88 removal of 78.0, 91.4, 94.4 and 96.6%, respectively, for 2, 4, 8 and 16 mM H_2O_2 (Fig. 8).

The increase of AR88 removal with the increase of H_2O_2 concentration could be explained by the increase of hydroxyl radical's production from the photolysis of H_2O_2 and due to the enhancement of the reactions between Fe^{2+} and H_2O_2 . However, when evaluating the pseudo first-order kinetic rate of AR88 degradation by the UV-A-Fenton process, it was

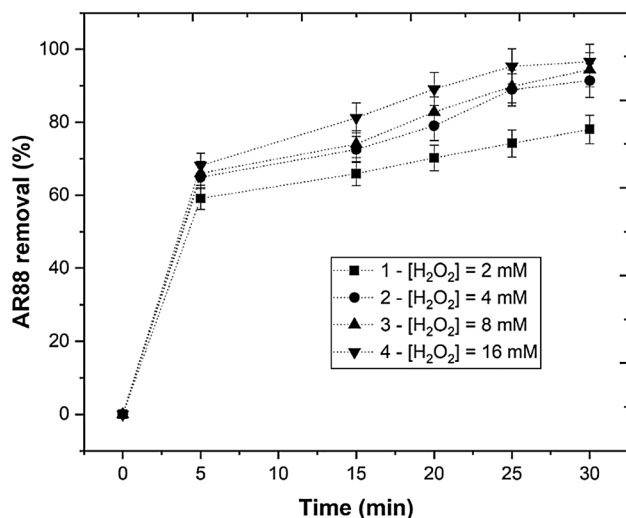


Fig. 8 Evolution of AR88 removal at different H₂O₂ concentrations (2–16 mM) in photo-Fenton experiments, under operational conditions, as follows: pH 3.0, [Fe²⁺]=0.15 mM, [AR88]=50 mg L⁻¹, agitation 350 rpm, T=298 K, radiation UV-A (365 nm), $I_{UV}=32.7 \text{ W m}^{-2}$, t=30 min

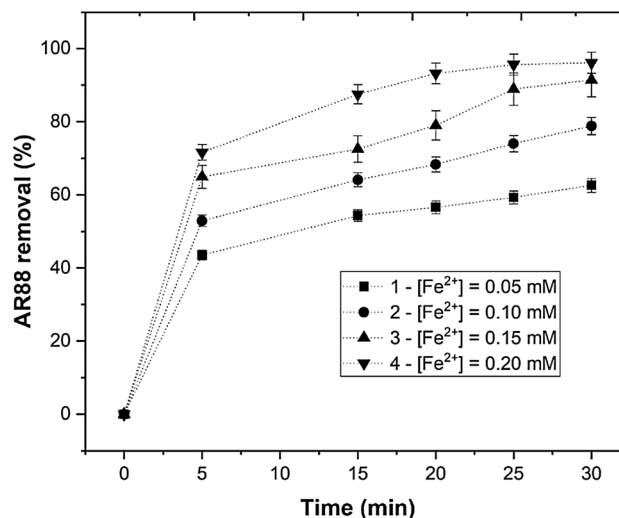
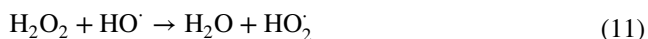


Fig. 9 Evolution of AR88 removal throughout the photo-Fenton experiments, using different Fe²⁺ concentration (0.05–0.20 mM). Operational conditions: pH 3.0, [H₂O₂]=4 mM, [AR88]=50 mg L⁻¹, agitation 350 rpm, T=298 K, radiation UV-A (365 nm), $I_{UV}=32.7 \text{ W m}^{-2}$, t=30 min

observed that increasing the H₂O₂ concentration to values higher than 4 mM ($k=8.32 \times 10^{-2} \text{ min}^{-1}$), had no significant improvement of the kinetic rate ($k=9.46 \times 10^{-2}$ and $10.64 \times 10^{-2} \text{ min}^{-1}$, respectively, for 8 and 16 mM H₂O₂). This could be attributed to the self-scavenging of HO[•] radicals by excess of H₂O₂ (Eqs. 11, 12) [60]. In addition, the application of 4 mM H₂O₂ reduces the consumption of H₂O₂ in comparison to the application of 8 and 16 mM. Therefore, based in these results, the concentration of 4 mM H₂O₂ was selected as the most efficient for UV-A-Fenton process.

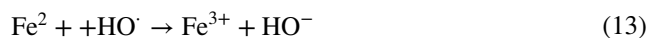


3.3.3 Influence of Fe²⁺ Concentration

The Fe²⁺ concentration is a very important parameter for the treatment of textile dyes by photo-Fenton process, due to (1) the cost of iron salt, (2) its influence on the needed irradiation time and (3) the residuals of iron in treated wastewaters and settled sludges, which can be harmful to the environment and requires further treatment to be separated [61, 62]. Therefore, in this section, it was performed the variation of Fe²⁺ concentration (0.05 to 0.20 mM) under the following operational conditions: pH=3.0, [H₂O₂]=4 mM,

[AR88]=50 mg L⁻¹, agitation 350 rpm, T=298 K, radiation UV-A (365 nm), $I_{UV}=32.7 \text{ W m}^{-2}$, t=30 min.

The results shown in Fig. 9, achieved an AR88 removal of 62.6, 78.8, 91.4 and 96.1%, respectively, for 0.05, 0.10, 0.15 and 0.20 mM Fe²⁺. With the application of 0.05 and 0.10 mM Fe²⁺, the amount of catalyst used was low, and as a consequence there was a low production of HO[•] radicals. With the application of 0.15 and 0.20 mM Fe²⁺, there was a higher production of HO[•] radicals, however, when observed the pseudo first-order kinetics ($k=8.32 \times 10^{-2} \text{ min}^{-1}$ and $k=10.54 \times 10^{-2} \text{ min}^{-1}$, respectively), the difference is not very significant. A similar effect was observed by Lucas and Peres [15], who observed that the addition of 0.20 mM Fe²⁺ had little differences regarding the addition of 0.15 mM Fe²⁺ in the treatment of RB5 by photo-Fenton process. The excess of iron observed with the application of 0.20 mM Fe²⁺, could have been responsible by scavenging reactions between Fe²⁺ and H₂O₂, as observed by Eq. 13 [63], as follows:



Therefore, based in these results, the concentration of 0.15 mM Fe²⁺ was selected as the best concentration.

3.3.4 Influence of Nitriloacetic Acid (NTA) Concentration

The UV-A-Fenton process, possess some limitations, such as the oxidation of Fe²⁺ to Fe³⁺, leading to the formation of ferric-hydroxyl complex (Fe(HO)²⁺) in the pH range 2.5–5.0, with a charge transfer band between 290 and 400 nm [64]. In order to overcome these limitations, it was tested in this work the addition of nitriloacetic acid (NTA) as a complexing agent. The strong ability of NTA as iron chelator represented by its stability or equilibrium constant (pK = 15.9 for Fe³⁺-NTA complexes and pK = 8.9 for Fe²⁺-NTA) makes it a reasonable candidate to be employed in this process [65, 66].

The concentration of NTA was varied (0.05–0.20 mM) under the operational conditions: with pH 3.0, [H₂O₂] = 4 mM, [Fe²⁺] = 0.15 mM, [AR88] = 50 mg/L, agitation 350 rpm, T = 298 K, radiation UV-A (365 nm), I_{UV} = 32.7 W m⁻², t = 30 min. The results showed an AR88 removal of 91.4, 88.1, 96.9, 88.9 and 68.5%, respectively, for 0.0, 0.05, 0.10, 0.15 and 0.20 mM NTA (Fig. 10). The application of 0.10 mM NTA (0.6:1 NTA:Fe²⁺ molar ratio) increased the efficiency of UV-A-Fenton process. These concentrations were lower than those applied by Zhang et al. [67], which required a NTA:Fe²⁺ molar ratio of 2:1 to degrade cyclohexanoic acid. The mechanism observed for NTA-Fenton process is as follows (Eqs. 14, 18) [21, 68]:

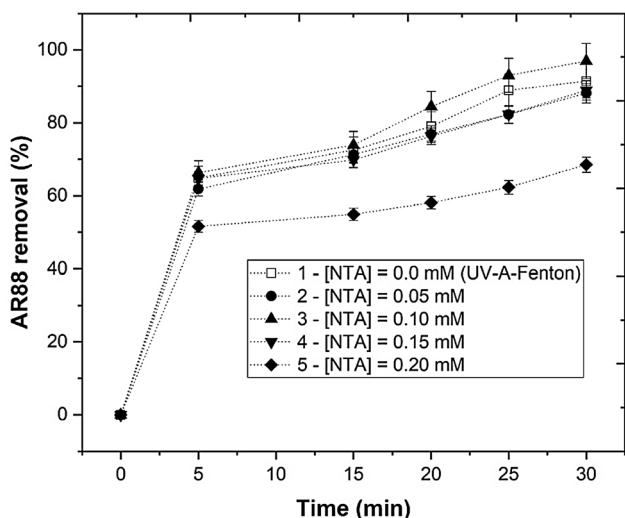
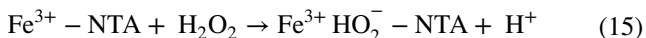
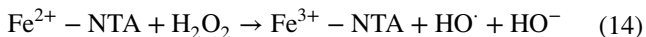
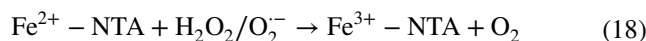
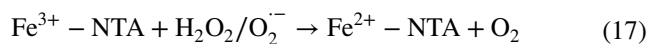
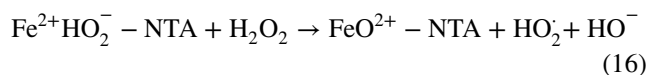
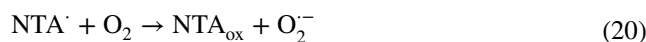
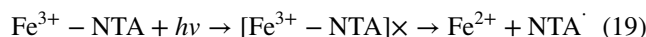


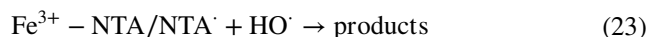
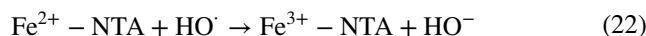
Fig. 10 Evolution of AR88 removal throughout the photo-Fenton experiments, using different NTA concentrations (0.00–0.20 mM). Operational conditions: pH 3.0, [H₂O₂] = 4 mM, [Fe²⁺] = 0.15 mM, [AR88] = 50 mg L⁻¹, gitation 350 rpm, T = 298 K, radiation UV-A (365 nm), I_{UV} = 32.7 W m⁻² = 30 min



With the application of UV-A radiation, the ferric complex formed with nitriloacetic acid (NTA), Fe³⁺-NTA, generated Fe²⁺ ions and NTA-free radicals (NTA[·]) by photoreduction through a ligand-to-metal charge transfer reaction (Eq. 19) [69]. The NTA radical also reacted with O₂ and hydroxyl ions to form superoxide radical anion (O₂⁻) and hydroxyl radicals (Eqs. 20, 21) [70], as follows:



With application of higher NTA:Fe²⁺ molar ratios it was observed a significantly decrease of AR88 degradation. These results were in agreement to De Laat et al. [71], who observed that when it is present an excess of NTA in solution, the NTA is mainly present as free NTA and may act as an HO[·] radical scavenger (Eqs. 22, 23), as follows:



Therefore, based in these results, 0.10 mM NTA was selected as the best NTA concentration.

3.3.5 Effect of AR88 Concentration

In this section, it was investigated the effect of initial dye concentration of aqueous solution, since pollutant concentration is an important parameter in wastewater treatment. The initial concentration of AR88 was varied from 25 to 100 mg L⁻¹ under the operational conditions, as follows: pH 3.0, [H₂O₂] = 4 mM, [Fe²⁺] = 0.15 mM, [NTA] = 0.10 mM, agitation 350 rpm, T = 298 K, radiation UV-A (365 nm), I_{UV} = 32.7 W m⁻², t = 30 min.

The results in Fig. 11, showed an AR88 removal of 99.5, 96.9, 82.6 and 68.4%, respectively, for 25, 50, 75 and 100 mg L⁻¹ AR88. From these results, it is possible to see that the extent of degradation decreased with the increase in the initial dye concentration. The increase of dye concentration increased the number of dye molecules and not the HO[·] radical concentration and therefore the AR88 removal percentage decreased. In addition, the high concentration of

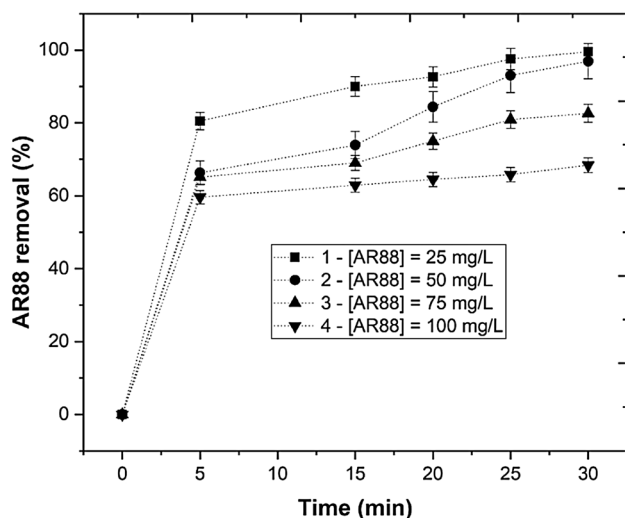


Fig. 11 Evolution of AR88 removal throughout the photo-Fenton experiments, using different AR88 concentration (25–100 mg L⁻¹). Operational conditions: pH 3.0, [H₂O₂]=4 mM, [Fe²⁺]=0.15 mM, [NTA]=0.10 mM, agitation 350 rpm, T=298 K, radiation UV-A (365 nm), $I_{UV}=32.7 \text{ W m}^{-2}$ = 30 min

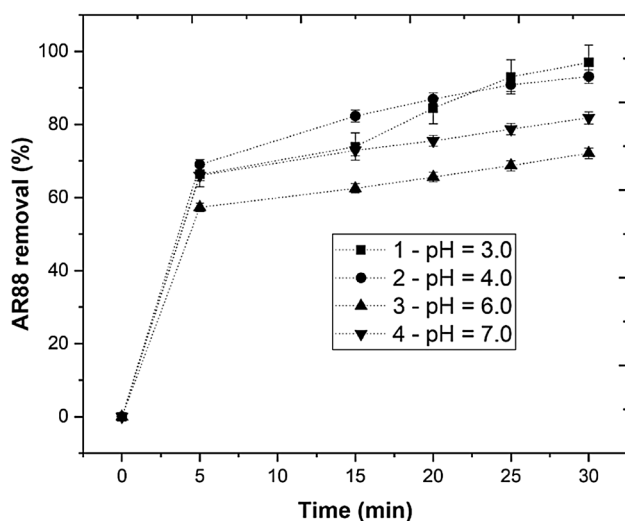


Fig. 12 Evolution of AR88 removal at different pH (3.0–7.0) in photo-Fenton experiments. Operational conditions: [H₂O₂]=4 mM, [Fe²⁺]=0.15 mM, [NTA]=0.10 mM, [AR88]=50 mg L⁻¹, agitation 350 rpm, T=298 K, radiation UV-A (365 nm), $I_{UV}=32.7 \text{ W m}^{-2}$, t=30 min

AR88, decreased the penetration of photons into the solution, consequently decreasing the production of HO[•] radicals [16]. Considering these results 50 mg/L AR88 was selected for the next step.

3.3.6 Effect of pH

The effect of pH on the rate of degradation of AR88 contaminant was investigated in the pH range of 3.0 to 7.0, under the operational conditions, as follows: [H₂O₂]=4 mM, [Fe²⁺]=0.15 mM, [NTA]=0.10 mM, [AR88]=50 mg L⁻¹, agitation 350 rpm, T=298 K, radiation UV-A (365 nm), $I_{UV}=32.7 \text{ W m}^{-2}$, t=30 min. An initial study showed that AR88 presents a pH of 6.12 ± 0.051 . The results showed an AR88 removal of 96.9, 93.1, 72.1 and 81.8%, respectively, for pH 3.0, 4.0, 6.0 and 7.0 (Fig. 12).

Although, the NTA has chelating properties to prevent the iron from precipitation at alkaline pH, results showed after 30 min of reaction a reduction of Fe²⁺ of 17.6, 15.2, 22.4 and 18.8%, respectively. However, when compared the UV-A-Fenton with UV-A-NTA-Fenton, it was observed a Fe²⁺ reduction of 27.2 and 17.6%, respectively. So, from this point of view, NTA successfully prevented the precipitation of iron at pH 3.0 as a result of the reaction between the Fe²⁺ with H₂O₂. This is due to the fact that NTA was decomposed into iminodiacetic acid (IDA) [72] and giving the formation of IDA-Fe²⁺ complex with low stability constant ($6.3 \times 10^5 \text{ M}^{-1} \text{ s}^{-1}$) [67], the iron was kept in solution longer.

Another point to be concerned, is the stability of iron at different pH, which is explained by the Pourbaix diagram (E–pH diagram). The Fe²⁺ precipitates at pH > 6.0 with the formation of Fe(OH)₂, while the Fe³⁺ generated in the reaction precipitates as iron oxyhydroxide (FeO(OH)) at pH 1.3. The oxyhydroxide species, are reduced to Fe²⁺ (aq) at pH < 6.0, while at pH > 6.0 there is the generation and precipitation of Fe(OH)₂ species [73]. Considering the lowest reduction of iron concentration, pH 3.0 was selected for the next step.

3.3.7 Effect of Irradiance Power

In this section it was evaluated the effect of the irradiation power in the degradation of AR88. The irradiation power was observed in the work of Ferreira et al. [74] to have a decisive effect on the degradation of RB5 by photo-Fenton process, therefore, the irradiation power was varied (22.9–32.7 W m⁻²), under the operational conditions, as follows: pH 3.0, [H₂O₂]=4 mM, [Fe²⁺]=0.15 mM, [NTA]=0.10 mM, [AR88]=50 mg L⁻¹, agitation 350 rpm, T=298 K, radiation UV-A (365 nm), t=30 min. The results showed a AR88 removal of 71.6, 84.8, 92.1 and 96.9%, respectively, for no radiation (NTA-Fenton), 22.9, 27.6 and 32.7 W m⁻² (Fig. 13). The addition of NTA improved the Fenton process from 63.1 to 71.6% AR88

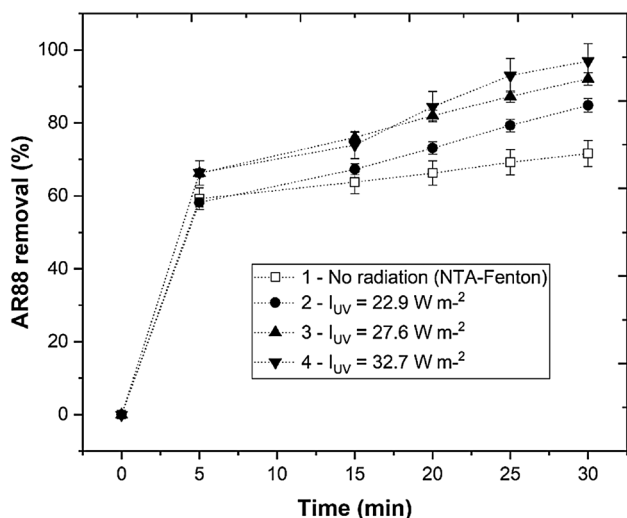


Fig. 13 Evolution of AR88 removal throughout the photo-Fenton experiments, with application of different irradiation power ($I_{UV}=0.0\text{--}32.7\text{ W m}^{-2}$). Operational conditions: pH 3.0, $[H_2O_2]=4\text{ mM}$, $[Fe^{2+}]=0.15\text{ mM}$, $[NTA]=0.10\text{ mM}$, $[AR88]=50\text{ mg L}^{-1}$, agitation 350 rpm, $T=298\text{ K}$, radiation UV-A (365 nm), $t=30\text{ min}$

removal, however, it was still insufficient and so irradiance was supplied in a UV-A-Fenton system. In order to understand the effect of the radiation in the rate of degradation of AR88, a plot was charted between $-\ln(AR88/AR88_0)$ vs t , in accordance to Eq. 4, can be further rearranged into $\ln[AR88]_t = -kt + \ln[AR88]_0$. Clearly, this chemical system is favored by high irradiances, considering that the highest kinetic rate of AR88 removal was obtained with the application of $I_{UV} = 32.7\text{ W m}^{-2}$ ($k = 95.62 \times 10^{-3}\text{ min}^{-1}$).

In a chemical photodegradation reaction, when a molecule decomposes after absorbing a light quantum, the quantum yield is the number of destroyed molecules divided by the number of photons absorbed by the system. The quantum yield (Φ) can be determined by Eq. 24, as follows [74]:

$$\Phi_{\text{Photodegradation}} = \frac{k}{2.303 \times I_{\lambda} \times \epsilon_{\lambda} \times l} \quad (24)$$

Table 4 Effect of irradiance power variation in pseudo first-order kinetics (k), half-life ($t_{1/2}$), photodegradation quantum yields $\Phi_{\text{Photodegradation}}$, electric energy per order (E_{EO}), and specific applied energy (E_{SAE}), with $[AR88]=50\text{ mg L}^{-1}$ and $V=250\text{ mL}$

Irradiance power (W m^{-2})	k (min^{-1})	$t_{1/2}$ (min)	$\Phi_{\text{Photodegradation}}$	E_{EO} $\text{kWh m}^{-3}\text{ order}^{-1}$	E_{ESA} $\text{kWh mol}^{-1}\text{ order}^{-1}$
0.0	$14.57 \times 10^{-3} \pm 1.63 \times 10^{-5}$ a	$47.56 \pm 5.33 \times 10^{-2}$ a	n.q	n.q	n.q
22.9	$40.05 \times 10^{-3} \pm 1.89 \times 10^{-5}$ b	$17.30 \pm 0.82 \times 10^{-2}$ b	$3.07 \times 10^7 \pm 1.45 \times 10^4$ a	$44 \pm 2.07 \times 10^{-2}$ a	351 ± 0.17 a
27.6	$56.90 \times 10^{-3} \pm 1.91 \times 10^{-5}$ c	$12.18 \pm 0.41 \times 10^{-2}$ c	$4.35 \times 10^7 \pm 1.47 \times 10^4$ b	$37 \pm 1.25 \times 10^{-2}$ b	298 ± 0.10 b
32.7	$95.62 \times 10^{-3} \pm 1.50 \times 10^{-5}$ d	$7.24 \pm 0.11 \times 10^{-2}$ d	$7.32 \times 10^7 \pm 1.15 \times 10^4$ c	$26 \pm 0.41 \times 10^{-2}$ c	210 ± 0.03 c

Means in the same column with different letters represent significant differences ($p < 0.05$) within each parameter (k , $t_{1/2}$, $\Phi_{\text{Photodegradation}}$, E_{EO} and E_{SAE}) by comparing irradiance powers. n.q.—not quantified

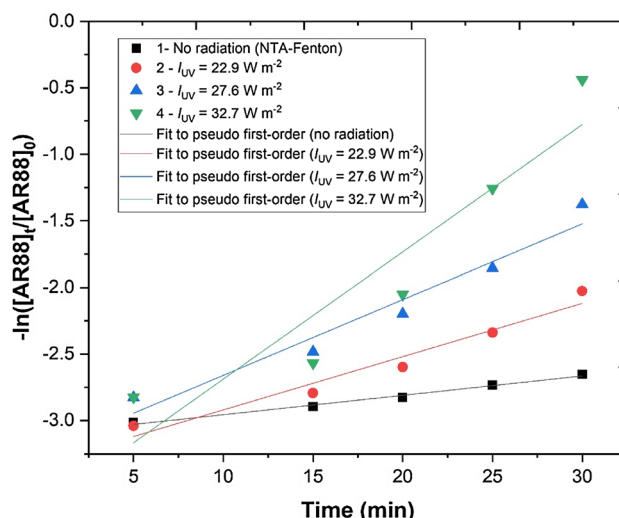


Fig. 14 Determination of pseudo first-order kinetic rate

where $\Phi_{\text{Photodegradation}}$ is the photodegradation quantum yield, k (s^{-1}) is the pseudo first-order rate constant, I_{λ} ($\text{Einstein L}^{-1}\text{ s}^{-1}$) is the light intensity at wavelength λ , ϵ_{λ} ($\text{cm}^{-1}\text{ mol dm}^{-3}$) is the molar absorptivity at wavelength λ , and l is the cell path length (cm) [75]. The results showed that increasing the light intensity increased significantly the quantum yield of the degradation process (Table 4), thus confirming that higher irradiation power leads to higher degradation of AR88 molecules.

Another aspect to take in consideration for the degradation of AR88 is the energy consumed in the photodegradation system, and so, the energy consumption was determined by application of electric energy per order (E_{EO}) and specific applied energy (E_{SAE}). With the determination of the kinetic rate (Fig. 14) significant differences were observed regarding energy consumption between the application of the different irradiation powers. In fact, with the increase of the irradiation power, the energy consumption decreased significantly (Table 4), achieving the lowest values with application of 32.7 W m^{-2} ($E_{EO} = 26\text{ kWh m}^{-3}\text{ order}^{-1}$ and $E_{SAE} = 210\text{ kWh mol}^{-1}\text{ order}^{-1}$).

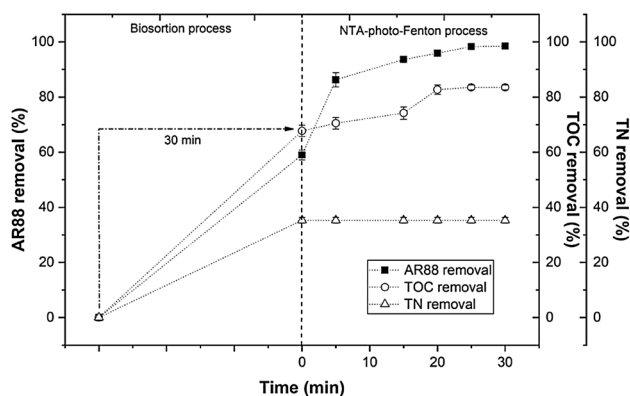


Fig. 15 Evolution of AR88, TOC and TN removal throughout the combined treatment of biosorption and photo-Fenton processes. Biosorption operational conditions: pH 3.0, [pollen]=3.0 g L⁻¹, [AR88]=100 mg L⁻¹, T=298 K, V=250 mL, agitation=350 rpm, t=30 min. Photo-Fenton operational conditions: pH 3.0 [H₂O₂]=4 mM, [Fe²⁺]=0.15 mM, [NTA]=0.10 mM, agitation 350 rpm, T=298 K, radiation UV-A (365 nm), I_{UV}=32.7 W m⁻², t=30 min

3.4 Combination of Biosorption and UV-A-NTA-Fenton Processes

Both adsorption and UV-A-NTA-Fenton processes were successively applied in the removal of AR88 from aqueous solution. Considering the AR88 concentration of 100 mg L⁻¹, both adsorption and UV-A-NTA-Fenton processes achieved alone 59.0 and 68.4% removal, respectively. In this section the UV-A-NTA-Fenton process was applied as a complement for the adsorption process, due to the capacity of the chemical process to degrade the molecules that weren't adsorbed by the pollen. Results showed an increase of the AR88 removal to 98.5% after 30 min of reaction (Fig. 15). A mineralization study was also performed, due to the fact that several intermediates molecules can be formed during the oxidation of the AR88 which could be toxic to the environment. The AR88 solutions presented an initial TOC and TN concentration of 52.2 mg C/L and 4.20 mg N/L. After the performance of adsorption process it was observed a reduction of 67.7 and 35.3%, respectively. The application of the UV-A-NTA-Fenton process further increase the mineralization of AR88, reaching 83.5% TOC removal after 30 min of reaction, however, as observed in Fig. 15, no further improvement in the removal of TN. It was also clear in this step that dye removal was much higher than TOC removal, which was in agreement to the findings of Lucas and Peres [16]. Finally, as an environmental concern, the wastewater pH is raised to 7, to precipitate the iron to be eliminated, thus the recovered water can be safely disposed.

4 Conclusions

The pollen of ADL can be successfully used for the removal of AR88 from aqueous solutions. The invasive ADL allows the textile dye bioadsorption and, at the same time, the decolourization of a problematic wastewater. To improve the global treatment, NTA was added to two well know AOPs–Fenton and UV-A-Fenton processes. The combined ADL biosorption and NTA-UV-A-Fenton system reaches an AR88 decolourization of 98.5% and a TOC removal of 83.5%. Thus, ADL pollen and NTA-UV-A-Fenton system can be a sustainable strategy to address the two main problems approached in this work: the invasive ADL control and the textile dye wastewater treatment.

Acknowledgements The authors are grateful for the financial support of the Project AgriFood XXI, operation No. NORTE-01-0145-FEDER-000041, and to the Fundação para a Ciência e a Tecnologia (FCT) for the financial support provided to CQVR through UIDB/00616/2020. Ana R. Teixeira also thanks the FCT for the financial support provided through the doctoral scholarship UI/BD/150847/2020.

Author Contributions ART and NJ: conceptualization. ART and NJ: methodology. NJ and ART: validation. ART and NJ: investigation. ART and NJ: writing-original draft preparation. ART, NJ, JRF, MSL and JAP: writing-review and editing. NJ, JRF, MSL and JAP: visualization. MSL and JAP: supervision. JAP: project administration. All authors have read and agreed to the published version of the manuscript.

Funding Open Access funding provided thanks to the CRUE-CSIC agreement with Springer Nature and to the Universidade de Vigo/ CISUG.

Declarations

Conflict of interest The authors declare no conflict of interest.

Open Access This article is licensed under a Creative Commons Attribution 4.0 International License, which permits use, sharing, adaptation, distribution and reproduction in any medium or format, as long as you give appropriate credit to the original author(s) and the source, provide a link to the Creative Commons licence, and indicate if changes were made. The images or other third party material in this article are included in the article's Creative Commons licence, unless indicated otherwise in a credit line to the material. If material is not included in the article's Creative Commons licence and your intended use is not permitted by statutory regulation or exceeds the permitted use, you will need to obtain permission directly from the copyright holder. To view a copy of this licence, visit <http://creativecommons.org/licenses/by/4.0/>.

References

- Bhatia D, Sharma NR, Singh J, Kanwar RS (2017) Biological methods for textile dye removal from wastewater: a review. *Crit Rev Environ Sci Technol* 47:1836–1876. <https://doi.org/10.1080/10643389.2017.1393263>

2. Khandare RV, Govindwar SP (2015) Phytoremediation of textile dyes and effluents: current scenario and future prospects. *Biotechnol Adv* 33:1697–1714. <https://doi.org/10.1016/j.biotechadv.2015.09.003>
3. Bankole PO, Adekunle AA, Govindwar SP (2018) Enhanced decolorization and biodegradation of acid red 88 dye by newly isolated fungus, *Achaetomium strumarium*. *J Environ Chem Eng* 6:1589–1600. <https://doi.org/10.1016/j.jece.2018.01.069>
4. Njoku VO, Foo KY, Asif M, Hameed BH (2014) Preparation of activated carbons from rambutan (*Nephelium lappaceum*) peel by microwave-induced KOH activation for acid yellow 17 dye adsorption. *Chem Eng J* 250:198–204. <https://doi.org/10.1016/j.cej.2014.03.115>
5. Song W, Gao B, Xu X et al (2016) Adsorption–desorption behavior of magnetic amine/Fe₃O₄ functionalized biopolymer resin towards anionic dyes from wastewater. *Bioresour Technol* 210:123–130. <https://doi.org/10.1016/j.biortech.2016.01.078>
6. Garg A, Mainrai M, Bulasara VK, Barman S (2015) Experimental investigation on adsorption of amido black 10B dye onto zeolite synthesized from fly ash. *Chem Eng Commun* 202:123–130. <https://doi.org/10.1080/00986445.2013.836636>
7. Şahin Ö, Kaya M, Saka C (2015) Plasma-surface modification on bentonite clay to improve the performance of adsorption of methylene blue. *Appl Clay Sci* 116:46–53. <https://doi.org/10.1016/j.clay.2015.08.015>
8. Jorge N, Teixeira AR, Lucas MS, Peres JA (2021) Combination of adsorption in natural clays and photo-catalytic processes for winery wastewater treatment. In: Abrunhosa M, Chambel A, Peppoloni S, Chaminié HI (eds) *Advances in geoethics and groundwater management: theory and practice for a sustainable development*. Springer, Cham, pp 291–294
9. Li W, Mu B, Yang Y (2019) Feasibility of industrial-scale treatment of dye wastewater via bio-adsorption technology. *Bioresour Technol* 277:157–170. <https://doi.org/10.1016/j.biortech.2019.01.002>
10. Casas MP, Conde E, Ribeiro D et al (2020) Bioactive properties of *Acacia dealbata* flowers extracts. *Waste Biomass Valorization* 11:2549–2557. <https://doi.org/10.1007/s12649-019-00639-4>
11. Martins F, Alegria C, Gil A (2016) Mapping invasive alien *Acacia dealbata* Link using ASTER multispectral imagery: a case study in central-eastern of Portugal. *For Syst* 25:13. <https://doi.org/10.5424/fs/2016253-09248>
12. Alves BA (1858) Plantas florestaes e de ornamento naturalisadas na Quinta do Lumiar. *Arch Rural Agric Artes e Sci Correl* 1:323–325
13. Lucas MS, Peres JA (2015) Removal of emerging contaminants by Fenton and UV-driven advanced oxidation processes. *Water Air Soil Pollut* 226:273. <https://doi.org/10.1007/s11270-015-2534-z>
14. Domínguez JR, Muñoz MJ, Palo P, González T, Peres JA, Cuerda-Correa EM (2014) Fenton advanced oxidation of emerging pollutants: parabens. *Int J Energy Env Eng* 5(89):1–10. <https://doi.org/10.1007/s40095-014-0089-1>
15. Lucas MS, Dias AA, Bezerra RM, Peres JA (2008) Gallic acid photochemical oxidation as a model compound of winery wastewaters. *J Env Sci Health Part A* 43(11):1288–1295. <https://doi.org/10.1080/10934520802177904>
16. Lucas MS, Peres JA (2006) Decolorization of the azo dye reactive black 5 by Fenton and photo-Fenton oxidation. *Dye Pigment* 71:236–244. <https://doi.org/10.1016/j.dyepig.2005.07.007>
17. Alalm MG, Tawfik A, Ookawara S (2015) Degradation of four pharmaceuticals by solar photo-Fenton process: kinetics and costs estimation. *J Environ Chem Eng* 3:46–51. <https://doi.org/10.1016/j.jece.2014.12.009>
18. Rojviroon T, Laobuthee A, Sirivithayapakorn S (2012) Photocatalytic activity of toluene under UV-LED light with TiO₂ thin films. *Int J Photoenergy* 2012:1–8. <https://doi.org/10.1155/2012/898464>
19. Natarajan K, Natarajan TS, Bajaj HC, Tayade RJ (2011) Photocatalytic reactor based on UV-LED/TiO₂ coated quartz tube for degradation of dyes. *Chem Eng J* 178:40–49. <https://doi.org/10.1016/j.cej.2011.10.007>
20. Bello MM, Raman AAA, Asghar A (2019) A review on approaches for addressing the limitations of Fenton oxidation for recalcitrant wastewater treatment. *Process Saf Environ Prot* 126:119–140. <https://doi.org/10.1016/j.psep.2019.03.028>
21. Ahile UJ, Wuana RA, Itodo AU et al (2020) A review on the use of chelating agents as an alternative to promote photo-Fenton at neutral pH: current trends, knowledge gap and future studies. *Sci Total Environ* 710:134872. <https://doi.org/10.1016/j.scitotenv.2019.134872>
22. Moreira FC, Boaventura RAR, Brillas E, Vilar VJP (2017) Electrochemical advanced oxidation processes: a review on their application to synthetic and real wastewaters. *Appl Catal B Environ* 202:217–261. <https://doi.org/10.1016/j.apcatb.2016.08.037>
23. Madhavan J, Maruthamuthu P, Murugesan S, Ashokkumar M (2009) Kinetics of degradation of acid red 88 in the presence of Co²⁺-ion/peroxomonosulphate reagent. *Appl Catal A Gen* 368:35–39. <https://doi.org/10.1016/j.apcata.2009.08.008>
24. Ghime D, Ghosh P (2018) Decolorization of diazo dye trypan blue by electrochemical oxidation: Kinetics with a model based on the Fermi's equation. *J Environ Chem Eng*. <https://doi.org/10.1016/j.jece.2018.11.037>
25. Das AB, Goud VV, Das C (2018) Adsorption/desorption, diffusion, and thermodynamic properties of anthocyanin from purple rice bran extract on various adsorbents. *J Food Process Eng* 41:e12834. <https://doi.org/10.1111/jfpe.12834>
26. Kasprzyk M, Gajewska M (2019) Phosphorus removal by application of natural and semi-natural materials for possible recovery according to assumptions of circular economy and closed circuit of P. *Sci Total Environ* 650:249–256. <https://doi.org/10.1016/j.scitotenv.2018.09.034>
27. Langmuir I (1916) The constitution and fundamental properties of solids and liquids. Part I. Solids *J Am Chem Soc* 38:2221–2295. <https://doi.org/10.1021/ja02268a002>
28. Gustafsson JP, Akram M, Tiberg C (2015) Predicting sulphate adsorption/desorption in forest soils: evaluation of an extended Freundlich equation. *Chemosphere* 119:83–89. <https://doi.org/10.1016/j.chemosphere.2014.05.067>
29. Wibowo E, Rokhmat M, Abdullah M (2017) Reduction of seawater salinity by natural zeolite (Clinoptilolite): adsorption isotherms, thermodynamics and kinetics. *Desalination* 409:146–156. <https://doi.org/10.1016/j.desal.2017.01.026>
30. Guimarães V, Rodríguez-Castellón E, Algarra M et al (2016) Influence of pH, layer charge location and crystal thickness distribution on U(VI) sorption onto heterogeneous dioctahedral smectite. *J Hazard Mater* 317:246–258. <https://doi.org/10.1016/j.jhazmat.2016.05.060>
31. Natarajan N, Kumar GS (2016) Effect of sips sorption isotherm on contaminant transport mechanism in fractured porous media. *KSCE J Civ Eng* 20:1714–1720. <https://doi.org/10.1007/s12205-015-1424-7>
32. Jovanovic DS (1969) Physical adsorption of gases I. Isotherms for monolayer and multilayer adsorption. *Kolloid-Zeitschrift Zeitschrift Fur Polym* 235:1203–1213. <https://doi.org/10.1007/BF01542530>
33. Maurer S (2000) *Prediction of Single Component Adsorption Equilibria*, 2nd edn. Herbert Utz Verlag, Germany
34. Jeppu GP, Clement TP (2012) A modified Langmuir-Freundlich isotherm model for simulating pH-dependent adsorption effects.

- J Contam Hydrol 129–130:46–53. <https://doi.org/10.1016/j.jconhyd.2011.12.001>
35. Chang R (2010) Chemistry, 10th edn. The McGraw-Hill Companies Inc, New York
 36. Durán A, Monteagudo JM, Carnicer A (2011) Photo-Fenton mineralization of synthetic apple-juice wastewater. Chem Eng J 168:102–107. <https://doi.org/10.1016/j.cej.2010.12.046>
 37. Bolton JR, Bircher KG, Tumas W, Tolman CA (2001) Figures-of-merit for the technical development and application of advanced oxidation technologies for both electric-and solar-driven systems (IUPAC Technical Report). Pure Appl Chem 73:627–637. <https://doi.org/10.1351/pac200173040627>
 38. Rodríguez-Chueca J, Amor C, Silva T et al (2017) Treatment of winery wastewater by sulphate radicals: HSO₃⁻/transition metal/UV-A LEDs. Chem Eng J 310:473–483. <https://doi.org/10.1016/j.cej.2016.04.135>
 39. Ferreira LC, Fernandes JR, Rodríguez-Chueca J et al (2020) Photocatalytic degradation of an agro-industrial wastewater model compound using a UV LEDs system: kinetic study. J Environ Manage 269:110740. <https://doi.org/10.1016/j.jenvman.2020.110740>
 40. Martin N, Bernard D (2018) Calcium signaling and cellular senescence. Cell Calcium 70:16–23. <https://doi.org/10.1016/j.ceca.2017.04.001>
 41. Marschner H, Römheld V (1994) Strategies of plants for acquisition of iron. Plant Soil 165:261–274. <https://doi.org/10.1007/BF00008069>
 42. Geider RJ, La RJ (1994) The role of iron in phytoplankton photosynthesis, and the potential for iron-limitation of primary productivity in the sea. Photosynth Res 39:275–301. <https://doi.org/10.1007/BF00014588>
 43. Olaleye AO, Tabi FO, Ogunkunle AO et al (2007) Effect of toxic iron concentrations on the growth of lowlands rice. J Plant Nutr 24:441–457. <https://doi.org/10.1081/PLN-100104971>
 44. Burzyński M, Kłobus G (2004) Changes of photosynthetic parameters in cucumber leaves under Cu, Cd, and Pb stress. Photosynthetica 42:505–510. <https://doi.org/10.1007/S11099-005-0005-2>
 45. Lisperguer J, Saravia Y, Vergara E (2016) Structure and thermal behavior of tannins from *Acacia dealbata* bark and their reactivity toward formaldehyde. J Chil Chem Soc 61:3188–3190. <https://doi.org/10.4067/s0717-97072016000400007>
 46. Baptista ATA, Silva MO, Gomes RG et al (2017) Protein fractionation of seeds of *Moringa oleifera* lam and its application in superficial water treatment. Sep Purif Technol 180:114–124. <https://doi.org/10.1016/j.seppur.2017.02.040>
 47. Carlo J, Jiménez J, Sofía A et al (2012) Extracción y evaluación de taninos condensados a partir de la corteza de once especies maderables de Costa Rica. Rev Tecnol en Marcha 25:15–22. <https://doi.org/10.18845/tm.v25i4.615>
 48. Lee W, Lan W (2006) Properties of resorcinol–tannin–formaldehyde copolymer resins prepared from the bark extracts of Taiwan acacia and China fir. Bioresour Technol 97:257–264. <https://doi.org/10.1016/j.biortech.2005.02.009>
 49. Vunain E, Mike P, Mpeketula G et al (2019) Evaluation of coagulating efficiency and water borne pathogens reduction capacity of *Moringa oleifera* seed powder for treatment of domestic wastewater from Zomba. Malawi J Environ Chem Eng 7:103118. <https://doi.org/10.1016/j.jece.2019.103118>
 50. Boulaadjoul S, Zemmouri H, Bendjama Z, Drouiche N (2018) A novel use of *Moringa oleifera* seed powder in enhancing the primary treatment of paper mill effluent. Chemosphere 206:142–149. <https://doi.org/10.1016/j.chemosphere.2018.04.123>
 51. Araújo CST, Alves VN, Rezende HC et al (2010) Characterization and use of *Moringa oleifera* seeds as biosorbent for removing metal ions from aqueous effluents. Water Sci Technol 62:2198–2203. <https://doi.org/10.2166/wst.2010.419>
 52. Saba B, Christy AD, Jabeen M (2016) Kinetic and enzymatic decolorization of industrial dyes utilizing plant-based biosorbents: a review. Environ Eng Sci 33:601–614. <https://doi.org/10.1089/ees.2016.0038>
 53. Sánchez-Martín J, Beltrán-Heredia J, Dávila-Acedo MA (2011) Optimum coagulant from *Acacia mearnsii* de Wild for wastewater treatment. Chem Eng Technol 34:2069–2076. <https://doi.org/10.1002/ceat.201100330>
 54. Hameed BH, Ahmad AA, Aziz N (2009) Adsorption of reactive dye on palm-oil industry waste: equilibrium, kinetic and thermodynamic studies. Desalination 247:551–560. <https://doi.org/10.1016/j.desal.2008.08.005>
 55. Beltrán-Heredia J, Sánchez-Martín J, Muñoz-Serrano A, Peres JA (2012) Towards overcoming TOC increase in wastewater treated with *Moringa oleifera* seed extract. Chem Eng J 188:40–46. <https://doi.org/10.1016/j.cej.2012.02.003>
 56. Guimarães V, Lucas MS, Peres JA (2019) Combination of adsorption and heterogeneous photo-Fenton processes for the treatment of winery wastewater. Environ Sci Pollut Res 26:31000–31013. <https://doi.org/10.1007/s11356-019-06207-6>
 57. Hage DS, Cazes J (2005) Handbook of Affinity Chromatography. CRC Press, Second
 58. Broom DP (2011) Hydrogen storage materials: the characterisation of their storage properties, 1st edn. Springer-Verlag, London
 59. Murrieta MF, Sirés I, Brillas E, Nava JL (2020) Mineralization of acid red 1 azo dye by solar photoelectro-Fenton-like process using electrogenerated HClO and photoregenerated Fe(II). Chemosphere 246:125697. <https://doi.org/10.1016/j.chemosphere.2019.125697>
 60. Malik PK, Saha SK (2003) Oxidation of direct dyes with hydrogen peroxide using ferrous ion as catalyst. Sep Purif Technol 31:241–250. [https://doi.org/10.1016/S1383-5866\(02\)00200-9](https://doi.org/10.1016/S1383-5866(02)00200-9)
 61. Alalm MG, Tawfik A, Ookawara S (2015) Comparison of solar TiO₂ photocatalysis and solar photo-Fenton for treatment of pesticides industry wastewater: operational conditions, kinetics, and costs. J Water Process Eng 8:55–63. <https://doi.org/10.1016/j.jwpe.2015.09.007>
 62. Alalm MG, Tawfik A (2013) Fenton and solar photo-Fenton oxidation of industrial wastewater containing pesticides. In: 17th International Water Technology Conference. pp 5–7
 63. Amor C, Lucas MS, Pirra A, Peres JA (2012) Treatment of concentrated fruit juice wastewater by the combination of biological and chemical processes. J Env Sci and Health Part A 47(12):1809–1817. <https://doi.org/10.1080/10934529.2012.689244>
 64. Faust BC, Hoigné J (1990) Photolysis of Fe (III)-hydroxy complexes as sources of OH radicals in clouds, fog and rain. Atmos Environ Part A Gen Top 24:79–89. [https://doi.org/10.1016/0960-1686\(90\)90443-Q](https://doi.org/10.1016/0960-1686(90)90443-Q)
 65. De LA, Dantas RF, Esplugas S (2014) Assessment of iron chelates efficiency for photo-Fenton at neutral pH. Water Res 61:232–242. <https://doi.org/10.1016/j.watres.2014.05.033>
 66. De LA, Dantas RF, Esplugas S (2015) Study of Fe (III)-NTA chelates stability for applicability in photo-Fenton at neutral pH. Applied Catal B, Environ 179:372–379. <https://doi.org/10.1016/j.apcatb.2015.05.025>
 67. Zhang Y, Klammerth N, Chelme-ayala P, El-din MG (2017) Comparison of classical fenton, nitrilotriacetic acid (NTA)-Fenton, UV-Fenton, UV photolysis of Fe-NTA, UV-NTA-Fenton, and UV-H₂O₂ for the degradation of cyclohexanoic acid. Chemosphere 175:178–185. <https://doi.org/10.1016/j.chemosphere.2017.02.058>
 68. Zhang Y (2016) Development and application of Fenton and UV-Fenton processes at natural pH using chelating agents for

- the treatment of oil sands process-affected water. University of Alberta, Edmonton
69. Stasicka Z (2011) Chapter 7 - transition metal complexes as solar photocatalysts in the environment: a short review of recent development. *Advances in inorganic chemistry*. Elsevier, pp 291–343
 70. Mejri A, Soriano-Molina P, Miralles-Cuevas S, Pérez JAS (2020) Fe³⁺-NTA as iron source for solar photo-Fenton at neutral pH in raceway pond reactors. *Sci Total Environ* 736:139617. <https://doi.org/10.1016/j.scitotenv.2020.139617>
 71. De Laat J, Dao YH, El Najjar NH, Daou C (2011) Effect of some parameters on the rate of the catalysed decomposition of hydrogen peroxide by iron (III)-nitrilotriacetate in water. *Water Res* 45:5654–5664. <https://doi.org/10.1016/j.watres.2011.08.028>
 72. Bunescu A, Besse-hoggan P, Sancelme M et al (2008) Fate of the nitrilotriacetic Acid-Fe (III) complex during photodegradation and biodegradation by *Rhodococcus rhodochrous*. *Appl Environ Microbiol* 74:6320–6326. <https://doi.org/10.1128/AEM.00537-08>
 73. Pesterfield LL, Maddox JB, Crocker MS, Schweitzer GK (2012) Pourbaix (E–pH–M) diagrams in three dimensions. *J Chem Educ* 89:891–899. <https://doi.org/10.1021/ed200423n>
 74. Ferreira LC, Lucas MS, Fernandes JR, Tavares PB (2016) Photocatalytic oxidation of reactive black 5 with UV-A LEDs. *J Environ Chem Eng* 4:109–114. <https://doi.org/10.1016/j.jece.2015.10.042>
 75. Rodríguez-Chueca J, Caldeira L, Fernandes JR, Tavares PB, Lucas MS, Peres JA (2015) Photocatalytic discolouration of Reactive black 5 by UV-A LEDs and solar radiation. *J Env Chem Eng* 3(4):2948–2956. <https://doi.org/10.1016/j.jece.2015.10.019>

Publisher's Note Springer Nature remains neutral with regard to jurisdictional claims in published maps and institutional affiliations.